Fracture Mechanics of Concrete Structures
Proceedings FRAMCOS-3
AEDIFICATIO Publishers, D-79104 Freiburg, Germany

ON NON-PLANAR FRACTURE IN CONCRETE

V. O. García-Álvarez, R. Gettu and I. Carol
School of Civil Engineering (ETSECCPB),
Universitat Politècnica de Catalunya, Barcelona, Spain.

Abstract
Non-planar fracture in eccentrically notched beams is studied using the size effect model and a mixed-mode cohesive crack model. It is seen that the crack path is independent of specimen size and that the brittleness of the failure is not influenced by its non-planarity. The cohesive crack analysis shows that the failure occurs mainly in mode I and is independent of the mode II fracture energy.
Keywords: Fracture, mixed-mode, size effect model, cohesive crack

1 Introduction

Non-planar fracture in concrete has often been considered as mixed-mode (combination of modes I and II) failure (Swartz et al., 1988; Bocca et al., 1991). However, several researchers have showed that in most of these cases, especially when the crack faces are not confined, the mode II component is negligible or non-existent (Jenq and Shah, 1988; Schlangen and van Mier, 1992). One of the geometries that have been studied is the center-loaded beam with an eccentric notch (Jenq and Shah, 1988).

In the present work, fracture tests were performed on three different sizes of center and eccentrically notched beams. The size effect method is applied to study the change in the brittleness due to the non-planar nature of the crack. The load versus crack opening responses are analyzed with a mixed-mode cohesive model to study the significance of the mode II component of the energy dissipation during the non-planar failure.

2 Experimental details

The composition of the concrete used has the proportions of cement:sand: gravel:water as 1:2.5:3.75:0.65. Spanish I/35A cement, limestone gravel (5-12 mm) and siliceous sand (0-5 mm) were used. Three batches (denoted A, B and C) of concrete were fabricated, and in each of them, nine beams were cast with the geometry shown in Fig. 1, three in each size, with $d = 80$, 160 and 320 mm, and thickness (b) of 50 mm.

Notches of length $l = 0.25d$ were cut in the beams with a diamond disc saw, with the eccentricities (e) of $0.625d$ ($0.25s$) for series A and $0.3125d$ ($0.125s$) for series B, respectively, and at midspan (e=0) for series C. The beams were tested at the age of 730 days, when the compressive strength was 27.3 MPa. All the specimens were stored in a fog room until testing.

The beam tests were conducted in a 1 MN INSTRON servohydraulic machine under closed-loop crack mouth displacement (CMD) control in three-point bending (3PB). Constant CMD rates were imposed such that the peak loads occurred at about 3 minutes. The load-CMD curve of each specimen was recorded; the curves are shown later with the fits of the cohesive crack model.

The crack paths observed on the surfaces of the specimens were recorded, and crack bands for each eccentricity were obtained from them. Figs. 2 a and b show the bands for $e \neq 0$, from which it can be concluded

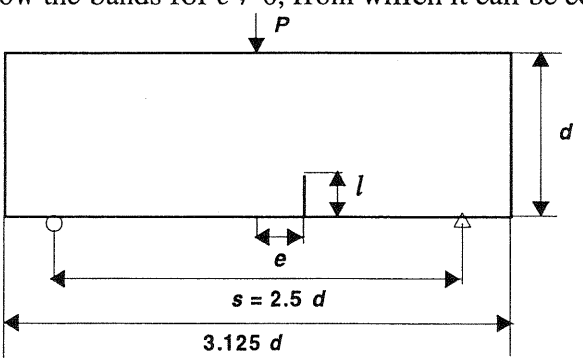

Fig. 1. Three point bend specimen

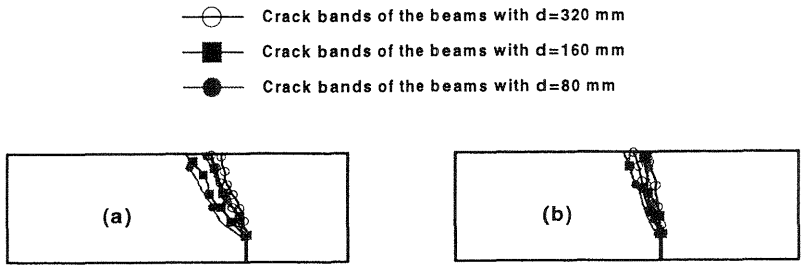

Fig. 2. Crack bands for (a) $e = 0.25s$ and (b) $e = 0.125s$

that the crack path does not depend significantly on the specimen size (i.e., they are geometrically similar). Note that the bands for different sizes have been normalized with respect to the beam depth for the comparison. This agrees with the results of other non-planar fracture tests in the literature (Bocca et al., 1991).

3 Application of the size effect model

The size effect model (SEM) of Bažant is based on the ductile-brittle transition of the failure mode of geometrically-similar fracture specimens, with an increase in size. It gives the size-dependence of the failure stress as (Bažant and Kazemi, 1990):

$$\sigma_N = \frac{B}{\sqrt{1+\beta}}; \qquad \beta = \frac{d}{d_0} \tag{1}$$

where $\sigma_N = P_u/bd$ is the maximum nominal stress, P_u is the peak load, d is a characteristic dimension of the specimen (here d is the beam depth), and B and d_0 are empirical parameters. The brittleness number, β, gives the proximity of the failure mode to ideal-brittle linear elastic fracture mechanics (LEFM) behavior; σ_N has a constant value (signifying ductile failure) at $\beta \to 0$ and is proportional to $d^{-1/2}$ (which corresponds to the LEFM failure) at $\beta \to \infty$. Parameters B and d_0 are obtained by fitting Eqn. 1 to the σ_N-values determined experimentally from different sizes of specimens. This form of the model is applicable as long as the crack paths are also geometrically similar.

In the case of mode I, the values of B and d_0 can be used to obtain material fracture parameters, which are theoretically independent of geometry effects (Bažant and Kazemi, 1990):

$$K_{Ic} = \frac{B}{\sqrt{d_0\, g(\alpha_0)}}; \qquad c_f = d_0 \frac{g(\alpha_0)}{g'(\alpha_0)}; \qquad G_f = \frac{K_{Ic}}{E} \tag{2}$$

where K_{Ic} = fracture toughness, c_f = effective fracture process zone length, G_f = fracture energy, E = modulus of elasticity (for plane stress), $\alpha_0 = l/d$, the relative notch length, g is the dimensionless energy release rate and g' its derivative with respect to the relative crack length. Functions g and g' depend on the specimen geometry and are obtained from LEFM analysis.

The SEM parameters were obtained by regression analysis of σ_N-values (from the peak loads obtained in the test and corrected for self-weight), using the Marquardt-Levenberg least-squares algorithm. The normalized test data are shown in Fig. 3, along with the fit. It can be seen that the SEM gives the trends for all the three eccentricities satisfactorily. More importantly, there is no shift in the position of the data with respect to the LEFM criterion indicating that the non-planar nature of the crack does influence the brittleness of the failure. The parameters given in Table 1, along with the coefficient of variation of the fits (ω), do not show any clear trend related to the notch eccentricity. The brittleness numbers for the three eccentricities are practically constant for each specimen size.

As mentioned earlier, the fracture parameters K_{Ic}, c_f and G_f can be obtained from the data of e = 0; the modulus of elasticity (E) of each specimen was computed from the initial load-CMD compliance using LEFM functions; the average E was 33.8 (±3.3) GPa. The values $g(\alpha_0)$ = 0.943 and $g'(\alpha_0)$ = 0.634 (for e = 0, α_0 = 0.25), obtained from finite element analysis, were used in Eqn. 2 to obtain K_{Ic} = 35.8 MPa-mm$^{1/2}$, c_f = 16 mm and G_f = 37.9 J/m^2.

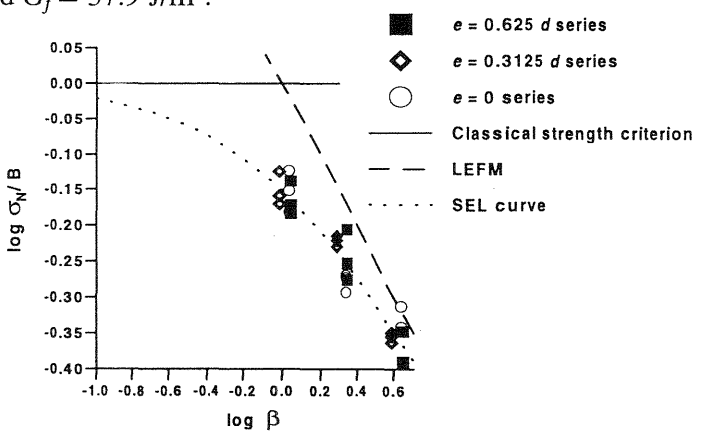

Fig. 3. Size effect plot for the three series

Table 1. Size effect model parameters

Series	e/d	B (MPa)	d_0 (mm)	ω	β		
					d=80mm	d=160mm	d=320mm
A	0.625	1.87	72	0.065	1.11	2.22	4.44
B	0.3125	1.33	82	0.045	0.98	1.96	3.92
C	0	1.36	74	0.079	1.08	2.16	4.32

4 Formulation of a cohesive crack model

The toughening effect of the fracture process zone (FPZ), which occurs in front of a progressing crack, is modeled as closing stresses in non-singular cohesive crack models (*cf.* Carol et al., 1997).

These generally have the following characteristics:

1. The behavior of the intact material follows a linear elastic stress-strain relation (without considering creep and other nonlinear material phenomena).
2. The crack propagation criterion (called the fracture criterion) can be expressed in terms of stresses and fracture parameters, as:
   $$F(\underline{S}, \underline{p}) = 0 \tag{3}$$
   where $\underline{S}$ is the stress vector and $\underline{p}$ is a vector consisting of material parameters such as tensile strength and fracture energy.
3. In a monotonically opening crack, $\underline{S}$ is the cohesive stress field in the FPZ, and a function of the crack opening vector ($\underline{\omega}$):
   $$\underline{S} = \underline{f}(\underline{\omega}) \tag{4}$$
   where $\underline{f}$ is the softening function.

In the present work, a cohesive crack model for non-planar tension-shear (mixed mode I+II) fracture is implemented with the discrete crack approach, where the discontinuity is modeled in the context of the finite element method through interface/joint elements (Rots, 1988; Carol et al., 1997). The fracture behavior is simulated through the constitutive law of the joint, which represents the cohesive crack stress-separation relation, and the fracture criterion F is expressed as (García-Álvarez, 1997):

$$F(\underline{S}, \underline{p}) = \tau^2 + tan^2\phi \ (\sigma - \chi)(2a - \sigma + \chi) = 0 \tag{5}$$

where σ and τ are the normal and shear stresses, $tan\phi$ represents the angle of friction between the crack faces, and χ and a are functions of the dissipated energy. Fig. 4 represents Eqn. 5 in a graphical form. In the case of Mode I, χ is the cohesive (tensile) stress. For the case of mixed mode fracture, an explicit softening function (as in Eqn. 4) cannot be

derived from Eqn. 5. Consequently, implicit stress-separation relations of the crack are developed in terms of the mode I and mode II components of the energy dissipation.

For the uncracked material, the constitutive law of the joint is linear elastic with stiffness coefficients D_n (normal to the joint element axis) and D_t (along the direction of the joint element axis). These coefficients must theoretically be infinite but in practice cannot be too large for avoiding oscillations in the stress profile (Gens et al., 1988).

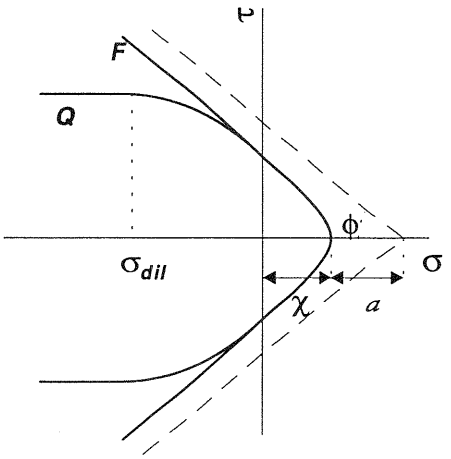

Fig. 4. Fracture criterion of the model

The opening (ω_n) and the sliding (ω_t) components of the crack separation can be expressed as the sums of the elastic displacement and the real crack opening as:

$$d\omega_n = d\omega_n^{el} + d\omega_n^{cr} \; ; \qquad d\omega_t = d\omega_t^{el} + d\omega_t^{cr} \tag{6}$$

where the components of the elastic displacement are:

$$d\omega_n^{el} = \frac{d\sigma}{D_n}; \qquad d\omega_t^{el} = \frac{d\tau}{D_t} \tag{7}$$

and the real crack opening is defined as:

$$d\omega_n^{cr} = d\lambda \frac{\partial Q}{\partial \sigma}; \qquad d\omega_t^{cr} = d\lambda \frac{\partial Q}{\partial \tau} \tag{8}$$

where $d\lambda$ is a multiplier (similar to that in plasticity theory), and $Q = F$ in tension and in compression is defined as:

$$\frac{\partial Q}{\partial \sigma} = 2 \tan^2 \phi \; (a + \chi - \sigma) \; f^{dil} \; ; \qquad \frac{\partial Q}{\partial \tau} = 2\tau \tag{9}$$

with

$$f^{dil} = \left(1 - \frac{\sigma}{\sigma_{dil}}\right)\frac{a+\chi}{a_0+\chi_0} \tag{10}$$

where σ_{dil} is the compressive stress beyond which there is no crack opening (or dilatancy). In the uncracked material, $\chi = \chi_0$ (tensile strength) and $a = a_0$ (related to the shear strength), which are parameters of Eqn. 9. The evolutions of χ and a depend on the energy dissipation (G) during crack propagation, which can be decomposed into the energies dissipated in mode I and mode II. G is expressed in a differential form as:

$$dG = dG^I + dG^{II} \tag{11}$$

In this formulation, the differential of the mode I component of G is defined as:

$$dG^I = \sigma\, d\omega_n^{cr} \quad if \quad \sigma \geq 0; \qquad dG^I = 0 \quad if \quad \sigma < 0 \tag{12}$$

and the mode II component as:

$$dG^{II} = \tau\, d\omega_t^{cr} \quad if \quad \sigma \geq 0;$$

$$dG^{II} = (|\tau| - |\sigma|\, tan\phi)\,|\, d\omega_t^{cr}\,| - |\sigma|\, d\omega_n^{cr} \quad if \quad \sigma < 0 \tag{13}$$

In the above equation, it can be seen that the G^{II} is the difference between the total energy dissipated in shear ($\tau d\omega_t^{cr}$), and the sum of energy dissipated due to friction ($|\sigma\ tan\phi\ d\omega_t^{cr}|$) and the energy dissipated due to dilatancy ($|\sigma d\omega_n^{cr}|$) (Willam, 1984; Weihe and Kröplin, 1995). Consequently, the dilatancy is treated in a manner similar to the way friction has been handled in the literature (Willam, 1984).

The evolutions of the parameters a and χ are given by:

$$a = a_0\left(1 - \xi_a\right); \qquad \chi = \chi_0\left(1 - \xi_\chi\right) \tag{14}$$

where

$$\xi_\chi = \frac{\int_0^{\omega^{cr}} dG^I}{G_F^I} + \frac{\int_0^{\omega^{cr}} dG^{II}}{G_F^{II}};$$

$$\xi_a = \frac{\int_0^{\omega^{cr}} dG^I + \int_0^{\omega^{cr}} dG^{II}}{G_F^{II}} \tag{15}$$

in which G_F^I and G_F^{II} are the fracture energies in modes I and II,

respectively. It can be seen in Eqns. 14 and 15 that in the case of pure mode I (i.e., $dG^{II} = 0$), when the FPZ is fully developed (i.e., $\int_0^{\omega^{cr}} dG^{I} = G_F^{I}$), the cohesive tensile stress vanishes. In pure mode II (i.e., $dG^{I} = 0$), both a and χ vanish when the FPZ is fully developed (i.e., $\int_0^{\omega^{cr}} dG^{II} = G_F^{II}$).

5 Application of the cohesive crack model

In order to apply the model formulated in the previous section to the 3PB specimen, the uncracked part is discretized with triangular and quadrilateral finite elements, while the crack path is represented by joint elements (as in Gens et al., 1988). The average crack paths obtained from the experimental bands (Fig. 2) were used. The computations were made with quadratic analysis, using the Gauss' 3×3 integration rule in quadrilateral elements and the 7-point Gauss' rule in triangular elements, and the 3-point Newton-Cotes' rule in the joints. The calculations take into account the weight of the concrete. In order to obtain stable solutions beyond the peak load, a displacement control method (Crisfield, 1994) is used for controlling the CMD (García-Álvarez, 1997).

In the analysis, $E = 33.8$ GPa, the Poisson ratio = 0.2 and the density of the concrete = 2350 kg/m^3. The elastic stiffness coefficients of the joints D_n and D_t are taken as 10^8 N/m. The parameter a_0 is chosen to be 9 MPa since this gives a ratio of 10 between the compressive and tensile strengths. In order to consider a reasonable relation between G_F^{II} and G_F^{I}, a parametric study of its influence was performed for the case of $e = 0.25s$. It was seen that the results were insensible to ratios in the range of $1 \le G_F^{II}/G_F^{I} \le 10$, and consequently the ratio was set as 1 for convenience. The other two parameters of the model (G_F^{I}, χ_0) are obtained by back-fitting the experimental load-CMD curves. The data for each eccentricity (i.e., for all the sizes) are analyzed together in order to reduce the uncertainty of the parameter set. Further details of the analyses can be found in García-Álvarez (1997).

The experimental data for each eccentricity and their optimum fits are shown in Figs. 5 a, b and c. The parameter set that gives satisfactory simulations of the load-CMD responses in all the cases is $G_F^{I} = 80$ J/m^2 and $\chi_0 = 3.5$ MPa. As expected (Planas and Elices, 1989), the value of G_F^{I} is larger than the fracture energy of the SEM.

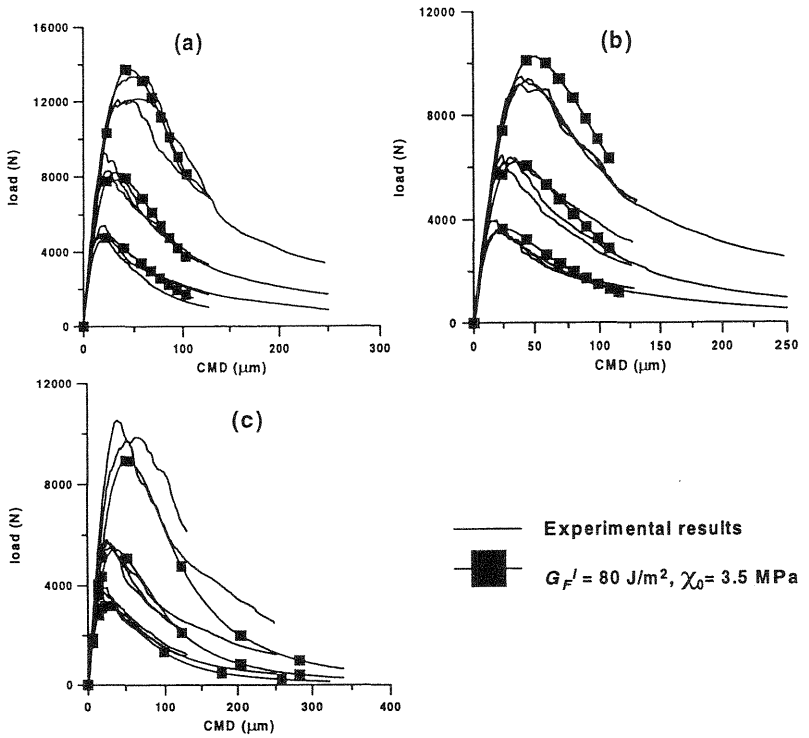

Fig. 5. Experimental data with the analytical fits for (a) $e = 0.25s$, (b) $e = 0.125s$ and (c) $e = 0$

As indicated by the parametric study of the influence of G_F^{II}/G_F^I, the mode II component of fracture is not significant in the cases analyzed here, as further confirmed from the comparisons of the evolutions of the total energy dissipation, G, and the mode I energy dissipation, G^I. In Figs. 6 a and b, these comparisons are given for $e = 0.25s$ and $e = 0.125s$, respectively, at three points along the crack path: point 1, at the notch tip; point 2, at a quarter of the crack length from the notch tip; and point 3, at the middle of the crack path. In all the cases, the evolutions of G and G^I practically coincide implying that G^{II} is negligible. This implies that the non-planar fracture studied here is basically a case of mode I failure and not of mixed-mode.

6 Conclusions

Tests of different sizes of geometrically similar beams with center and

eccentric notches have been performed. As expected, the crack paths in the cases of eccentric notches are non-planar and are observed to be independent of the specimen size. The data have been analyzed with the size effect model (SEM) and a mixed-mode cohesive crack model implemented in a finite element code.

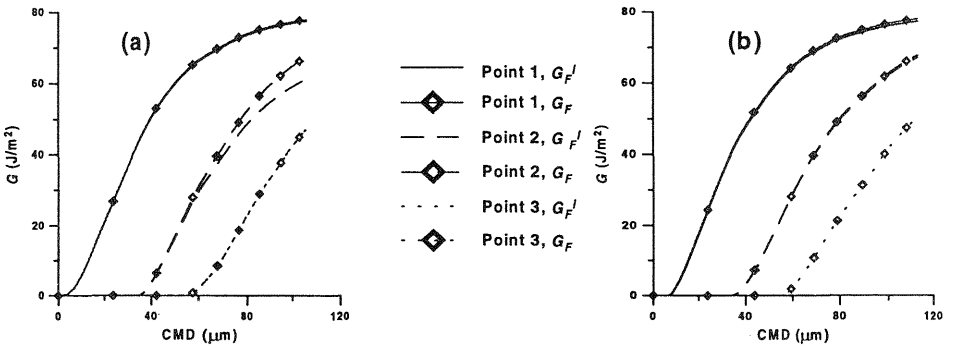

Fig. 6. Evolutions of the total and mode I energy dissipation

The size effect analyses indicate that the brittleness of the failure does not change due to the eccentricity of the notch and the non-planar nature of the crack path.

The cohesive crack analysis show that the mode II component of the energy dissipation is negligible for this type of failure, and that the failure is primarily in mode I. The fracture energy used in this model is much higher than the value obtained from the SEM, as expected.

7 Acknowledgments

Partial funding from Spanish CICYT project MAT96-0967 and DGES project PB96-0500, and a CIRIT grant AR91-420 to the UPC.

8 References

Bažant, Z.P. and Kazemi, M.T. (1990), Determination of fracture energy, process zone length and brittleness number from size effect, with application to rock and concrete. **Int. J. Fract.**, 44, 111-131.

Bocca, P., Carpinteri, A. and Valente, S. (1991) Mixed mode fracture of

concrete, **Int. J. Solids Structures**, 27, 1139-1153.

Carol, I. Prat, P.C. and López, C.M. (1997) Normal/shear cracking model: application to discrete crack analysis, **J. Engng. Mech.**, 123, 765-773.

Crisfield, M.A. (1994) **Non-linear finite element analysis of solids and structures**, Vol. 1, John Wiley & Sons, New York.

García-Álvarez, V.O. (1997) **Study of Mixed Mode Fracture in Quasi-brittle Materials** (in Spanish), Doctoral thesis, School of Civil Engineering, Universitat Politècnica de Catalunya, Barcelona.

Gens, A., Carol, I. and Alonso, E.E. (1988) An interface element formulation for the analysis of soil-reinforcement interaction, **Computers and Geotechnics**, 7, 133-151.

Jenq, Y.S. and Shah, S.P. (1988) Mixed-mode fracture of concrete, **Int. J. Fract.**, 38, 123-142.

Planas, J. and Elices, M. (1989) Size effect in concrete structures: Mathematical approximations and experimental validation, **Cracking and Damage,** Elsevier, London, 462-476.

Rots, J.G. (1988) **Computational modelling of concrete fracture**, Doctoral thesis, Delft University of Technology, Delft.

Schlangen, E. and van Mier, J.G.M. (1992) Fracture modelling of granular materials, **Mat. Res. Soc. Symp. Proc.**, 278, 153-158.

Swartz, S.E., Lu, L.W., Tang, L.D. and Refai, T.M.E. (1988) Mode II fracture-parameter estimates for concrete from beam specimens, **Expt. Mech.**, 28, 146-153.

Weihe, S. and Kröplin, B. (1995) The fictitious crack concept in the mechanics of composites, **Computational Plasticity (COMPLAS IV),** Pineridge Press, New Jersey.

Willam, K. J. (1984) Experimental and computational aspects of concrete fracture, in **Computer aided analysis and design of concrete structures,** Pineridge Press, New Jersey, 33-70.